Journal of Inorganic Biochemistry 194 (2019) 7–18

Contents lists available at ScienceDirect

Journal of Inorganic Biochemistry

journal homepage: www.elsevier.com/locate/jinorgbio

Diclofenac conjugates with biocides through silver(I) ions (CoMeD's); Development of a reliable model for the prediction of anti-proliferation of NSAID's-silver formulations.

Christina N. Banti[a,*], Antonios G. Hatzidimitriou[b], Nikolaos Kourkoumelis[c,*], Sotiris K. Hadjikakou[a,*]

[a] Inorganic Chemistry Laboratory, Department of Chemistry, University of Ioannina, 45110 Ioannina, Greece
[b] Department of Chemistry, Aristotle University of Thessaloniki, Thessaloniki 54124, Greece
[c] Medical Physics Laboratory, Medical School, University of Ioannina, Greece

ARTICLE INFO

Keywords:
Bioinorganic chemistry
Drugs development
Diclofenac
Silver(I)
Cytotoxicity
Regression analysis

ABSTRACT

The conjugation of diclofenac (DICLH), a Non-Steroidal Anti-inflammatory Drug (NSAID), with biocides such as dimethyl sulfoxide (DMSO) and triphenylphosphine (TPP), through silver(I) ions, results into the chemical $[Ag_n(DICL)_n(L)_m]_k$ (L = DMSO and n = 2, m = 2, k = infinite (**1**); L = TPP and n = 1, m = 2, k = 1 (**2**)). The compounds were characterized by m.p., FT-IR, UV–vis and ^{1}H NMR spectroscopic techniques. The crystal and molecular structures of **1–2** were determined by X-ray crystallography. The in vitro cytotoxic activity of **1–2** against the human breast adenocarcinoma cancer cells MCF-7 (hormone dependent) and MDA-MB-231 (hormone independent) reveals that the **1** inhibits the MCF-7 rather than the MDA-MB-231 cells, suggesting hormone mimetic behaviour. Compound **2** inhibits both cancerous cell lines, stronger than cisplatin. Both compounds inhibit MCF-7 cells migration. Compounds **1–2**, exhibit, lower toxicity against fetal lung fibroblast (MRC-5) cells than cisplatin. Their genotoxicity was evaluated on MRC-5 cells. The molecular mechanism of **1–2** against MCF-7 cells was clarified by (i) their cell cycle arrest study (ii) their mitochondrial membrane permeability (iii) their binding affinity towards Calf Thymus (CT)-DNA and (iv) their inhibitory activity against the enzyme lipoxygenase (LOX). Regression analysis of the data obtained for $[Ag(NSAID)(Ar_3P)_m]$ (NSAID = p-hydroxy-benzoic acid (p-HO-BZAH), salicylic acid ($SALH_2$), aspirin (ASPH), naproxen (NAPRH), nimesulide (NIMH); L = TPP, Tri(p-tolyl)phosphine (TPTP), Tri(o-tolyl)phosphine (TOTP), Tri(m-tolyl)phosphine (TMTP); m = 2 or 3) and $[Ag(DICL)_2(DMSO)_2]_k$ (k = infinite) was performed. Considering the biological results (IC_{50}) as dependent variable a theoretical equation is obtained for these compounds. The calculated IC_{50} values are compared satisfactorily with the corresponding experimental inhibitory activity of the complexes.

1. Introduction

The nonsteroidal anti-inflammatory drugs (NSAIDs) have been reported to accord protection against many types of tumors like colon, oesophagus and breast cancer [1]. The strong antiproliferative activity of NSAIDs is linked with mitochondrial dysfunction and apoptosis [2–6]. It is notified that the main cell organelle targeted from NSAIDs is mitochondrion where the inflammation mechanism is mainly operated. Moreover, coordination of NSAIDs to metal ions enhances their activities, and the formed metallodrugs display a range of biological potency inaccessible to the original NSAID ligands [7]. Biological variations in the activity of these compounds are attributed to the different NSAIDs-silver(I) moieties [7,8]. Such molecular species interact with DNA and inhibit the enzyme lipoxygenase (LOX), which is mainly distributed in mitochondrion [2–4]. The use of the NSAID diclofenac, is already approved for treatment of actinic keratosis (a precancerous scaly, patch of thick crusty skin), whereas others NSAIDs, such as acetylsalicylic acid and celecoxib are used in clinical trials, for breast or colon carcinoma, respectively [9].

The medical applications of DMSO originate from its anti-inflammatory, antioxidant and analgesic activities [10]. Above all, however, DMSO penetrates membranes and therefore it is often used as a carrier for pharmaceuticals into cells [11]. Triphenylphosphonium ($TPPH^+$), on the other hand, penetrates the mitochondrial membrane due to its lipophilicity and its stable cationic charge [12]. Thus, the combination of a NSAID with either a penetrator or a

* Corresponding authors.
E-mail addresses: cbanti@uoi.gr (C.N. Banti), nkourkou@uoi.gr (N. Kourkoumelis), shadjika@uoi.gr (S.K. Hadjikakou).

https://doi.org/10.1016/j.jinorgbio.2019.01.020
Received 8 December 2018; Received in revised form 15 January 2019; Accepted 17 January 2019
Available online 17 February 2019
0162-0134/

mitochondriotropic agent is expected to result in chemical formulations able for cell membranes transpiration, and through this, to interact with DNA or mitochondrion, where they can cause damages leading cells to apoptosis.

Cisplatin and its analogues, anti-cancer drugs in clinical use, on the other hand, are known to bind various cellular components like DNA, RNA, proteins, and membrane phospholipids. Although their main target leading cells to death through apoptosis is genomic DNA [13,14], other targets than DNA, however may be also important for these agents [13,14]. The important and strong side effects of these series of drugs, however initiated the development of the second and third generation of anticancer formulations with milder side effects and higher selectively to cancerous cells.

One of new areas that our group is involving for the discovery of new synergistic therapeutic modalities is the Conjugation of Metals with specific classes of Drugs (CoMeD). By bringing two different agents together through a metal ion as linker, this technology provides the opportunity for synergistic effects [2–4,15–22]. Aiming on the development of new chemical formulations which are targeting to mitochondrion, two new compounds were synthesized by the conjugation of diclofenac (DICLH), with dimethyl sulfoxide (DMSO) and triphenylphosphine (TPP) (Scheme 1), through silver(I) ions, $[Ag_n(DICL)_n(L)_m]_k$ (L = DMSO and $n = 2$, m = 2, k = infinite (**1**); L = TPP and $n = 1$, m = 2, k = 1 (**2**)). The compounds **1–2** were characterized by m.p., FT-IR, UV–vis and ^{1}H NMR spectroscopic techniques and X-ray crystallography. The in vitro cytotoxic activity of **1–2** was tested against MCF-7 (hormone depended) and MDA-MB-231 (hormone independent). The cell migration assay was employed in order to verify the prevention of MCF-7 cells migration which is essential for the anti-metastatic agents. The toxic effect caused by **1–2** was surveyed against normal human fetal lung fibroblast cells (MRC-5 cells), while their genotoxicty was evaluated against MRC-5 cells by the micronucleus assay using fluorescence microscopy.

The mechanism of the new small molecules against cancer cells was studied by the mean of: (i) cell cycle arrest (ii) permeability of the mitochondrial membrane test (iii) their affinity for Calf Thymus (CT)-DNA and (iv) their inhibitory activity against the enzyme lipoxygenase (LOX). Structure activity relationship (SAR) was made by comparing the activity of **1–2** with the corresponding one of others homologues heteroleptic silver(I) compounds of NSAID and triarylphosphines (Ar3P).

2. Results and discussion

2.1. General aspects

Crystals of **1** were grown from the reaction between silver nitrate and diclofenac sodium in DMSO solution, while crystals of **2** were formed upon treatment of the DMSO solution of **1** solution with TPP (Scheme 2). The crystals of **1–2** are stored in darkness at room temperature.

2.2. Solid state studies

2.2.1. Crystal and molecular structures of $[Ag_2(DICL)_2(DMSO)_2]_n$ (1), $[Ag(DICL)(TPP)_2]$ (2)

Molecular diagrams of **1–2** along with their selected bond distances and angles are shown in Figs. 1–2.

Compound **1** is polymeric. One 8-member ring constitutes the building block of the polymer (Fig. 1A). Two four coordinated silver atoms are bridged together by two carboxylic groups from two diclofenac ligands (Ag1-O2 = 2.533(4), Ag1-O1_d = 2.218(4) Å respectively) leading to Ag···Ag1_a bonding interaction of 2.8451(11) Å (Fig. 1A). The coordination sphere of Ag(I) centres is completed by one O from DMSO. The Ag···Ag interactions, known as argentophilicity for silver, lead to metalloaromaticity in the ring, which therefore adds further stabilization to the ring. Two 8-member rings are bridged together by two Ag1-O10# = 2.533(4)Å forming a 4-member ring (Fig. 1B), while the tetrahedron around silver is now completed. Finally, an architecture of waveform ribbon is established (Fig. 1C).

Two oxygen atoms from a chelating carboxylic group (Ag1-O1 = 2.4208(15), Ag1-O2 = 2.4778(16) Å) and two phosphorus atoms from two TPP ligands (Ag1-P1 = 2.4147(6), Ag1-P2 = 2.4322(6) Å) complete the tetrahedral conformation around the Ag(I) ion in the structure of **2** (Fig. 2).

The Ag—O and Ag—P bond lengths of both **1** (Ag1-O2 = 2.533(4), Ag1-O1_d = 2.218(4)) and **2** (Ag1-O1 = 2.4208(15), Ag1-O2 = 2.4778(16) Å and Ag1-P1 = 2.4147(6), Ag1- P2 = 2.4322(6) Å) are in the range of the already known ones. The average intra-molecular Ag—O and Ag—P distances of the compounds synthesized by our group ($[Ag(p\text{-}HO\text{-}BZAH)(TPP)_2]$ (p-HO-BZAH = p-hydroxy-benzoic acid), [16], $[Ag(SALH)(TPP)_2]$ ($SALH_2$ = salicylic acid) [15], $\{[Ag(ASP)(TPP)_3](DMF)\}$ (ASPH = aspirin) [15], $\{[Ag(NAPR)(TPP)_3](H_2O)\}$ (NAPRH = naproxen) [3], $[Ag(NIM)(TPP)_2]$ (NIMH = nimesulide) [2], $[Ag(NIM)(TPTP)_2]$ (TPTP = Tri(p-tolyl)phosphine) [2],[Ag(NIM)(TOTP)] (TOTP = Tri(o-tolyl)phosphine) [2], $[Ag(NAPR)(TPTP)_2]$ [3], $[Ag(SALH)(TPTP)_2]$ [4], $[Ag(SALH)(TMTP)_2]$ (TMTP = Tri(m-tolyl) phosphine) [4] and $[Ag(p\text{-}HO\text{-}BZAH)(TPTP)_2]$ [4]) are 2.459 ± 0.038 and 2.444 ± 0.019 Å respectively.

Hydrogen bonding interactions (N1[H11]···Cl2 = 2.964(5) Å and N1[H11]···O1 = 3.065(6)Å) lead to 3D polymeric assembly in **1**. In **2** the N1[H11]···Cl1 = 3.003(2) and N1[H11]···O2 = 2.838(2) bonding interactions are intramolecular and play no much significant role in the stabilization of this compound.

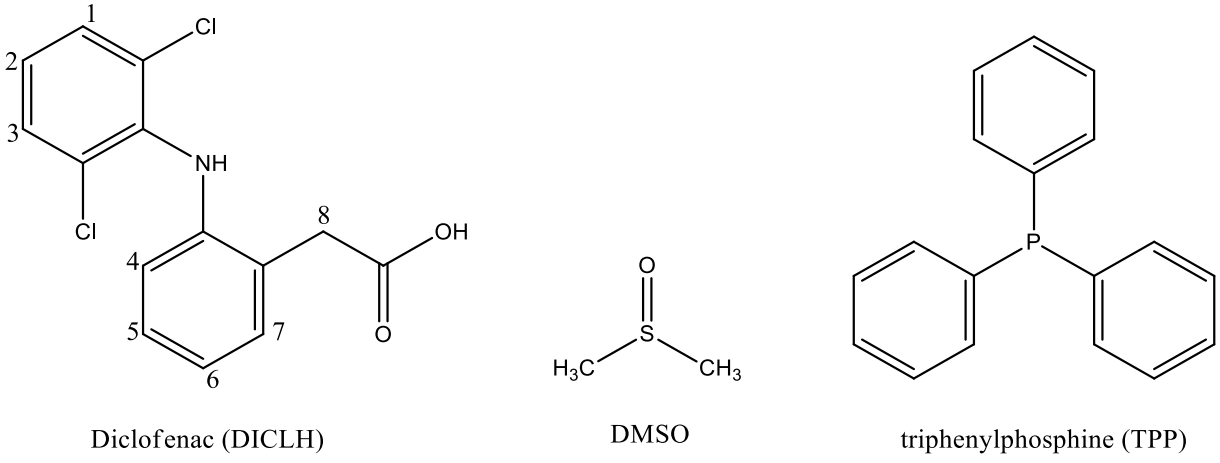

Scheme 1. Ligands used.

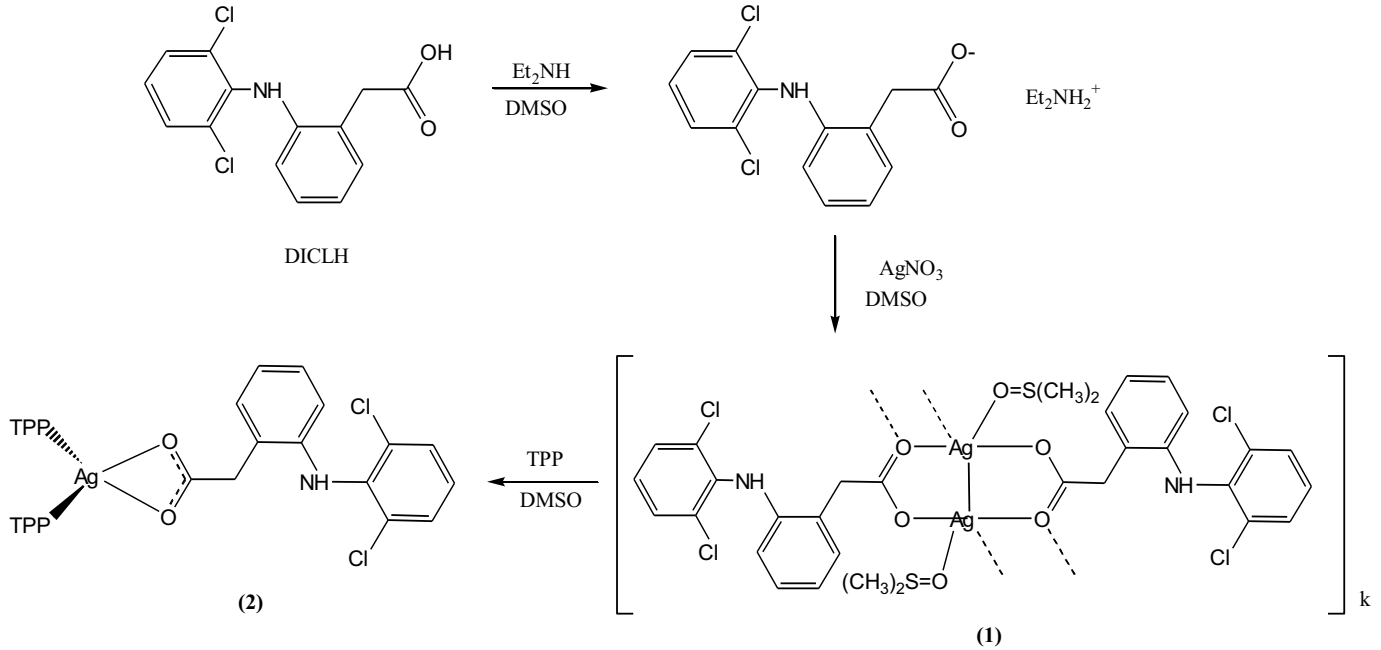

Scheme 2. Synthetic route.

The geometry around four coordinated metal ions is either tetrahedral, seesaw or square planar. According to Yang et al. [23] criterion when the parameter τ4 (Eq. (1)) is equal to 0 the geometry is square planar, when it is unity the geometry is tetrahedron, while when t4 equals to 0.43 the geometry is ideal seesaw. In case of **1** the t4 value is 0.47, while the corresponding τ4 value for **2** is 0.80. Thus almost ideal seesaw geometry and a disorder tetrahedral one is concluded for **1** and **2**.

$$\hat{o}4 = \frac{360 - (a + b)}{360 - 2^{*}\grave{e}} \quad (1)$$

Equation for the geometry definition of four coordinated, metal centers, [23]; a and b are the greatest angles around the metal; θ = 1 / (cos(−1/3)) ≈ 109.5.

2.2.2. Vibrational spectroscopy

In order to confirm the homogeneity of the samples, FT-IR spectra were recorded using KBr discs. The vibration bands at 1570 and 1470 cm^{-1} in the IR spectrum of diclofenac sodium salt (Fig. S1) are assigned to the ν_{as}(COO–) and ν_s(COO–), respectively [24]. These bands are shifted at 1574 and 1470 cm^{-1} respectively in IR spectrum of **1** (Fig. S2) and at 1574 and 1480 cm^{-1} respectively in case of **2** (Fig. S3). The Δν difference values of **1–2** (104 cm^{-1} (**1**) and 94 cm^{-1} (**2**)). However, monodentate coordination of the carboxylic group results in a significantly higher difference values Δν than those observed for the ionic compounds of the ligand [25], while when the ligand chelates, the Δν is considerably smaller than that observed for its ionic compounds. For asymmetric bidentate coordination, the values are in the range of monodentate one [25]. When the −COO– group bridges metal ions, the Δν values are higher than that of the chelating mode and nearly the same as that observed for ionic compounds [25]. Since the corresponding Δν value of sodium diclofenac salt is 104 cm^{-1} the carboxylic group coordinates in bridging manner at **1** and it chelates in **2** (Δν values are 104 (**1**) and 90 (**2**) cm^{-1}) in accordance to the structures refined X-ray diffraction data. The vibration bands of C−Cl and C−N bonds in the FT-IR spectrum of diclofenac sodium, are observed at 766 and 1306 cm^{-1} respectively and they are not shifted upon coordination (Figs. S2–S3) [24,26]. The bands at 512–481 cm^{-1} in the IR spectrum of **2** are attributed to the ν(C–P) vibrations of triphenylphosphine, confirming the coordination of the TPP (Fig. S4) [2]. The corresponding vibration bands of the free TPP are observed at 521–500 cm^{-1} (Fig. S3).

2.3. Solution studies

2.3.1. Stability of 1–2 in solvent media

The stability of **1–2** in DMSO/water solutions was checked by Uv-vis (Figs. S5–S6) and ^{1}H NMR spectroscopy (Figs. S7–S8) for a period of 48 h, since the biological experiments requires this incubation period. No changes were observed between the spectra recorded initially and those after 48 h.

2.3.2. ^{1}H NMR studies

The retention of the structures of **1–2** in DMSO solution was confirmed by ^{1}H NMR spectroscopy (Figs. S9–S10). This is precondition for the biological experiments since DMSO stock solutions of **1–2** were used. The resonance signal in the ^{1}H NMR spectrum of diclofenac sodium in DMSO-d_6 at 10.618 ppm is attributed to the amide proton H[N] of diclofenac [27,28]. This signal is shifted at 9.193 (**1**) and 9.745 (**2**) ppm, respectively in the spectra of **1–2** (Figs. S9–S10). The resonances signals at 6.212–7.452 ppm in the spectrum of the sodium salt of DICL are attributing to the aromatic protons H[Ar] [27,28]. The doublet signal at 7.452–7.432 ppm is attributed to H[^{1,3}C] of the 2,6-dichlorophenyl phenyl ring of diclofenac sodium. This signal is shifted in the spectra of **1–2** at 7.487–7.471 (**1**) and 7.421–7.405 (**2**) ppm respectively (Figs. S9–S10). The resonance signal of H[^{5,7}C] of the phenyl acetate ring of diclofenac sodium is observed at 7.071–7.014 ppm and it is shifted in the spectra of **1–2** at 7.134–7.088 (**1**) and 7.116–7.106 (**2**) ppm (Figs. S9–S10). The triplet signal of H[^{2}C] of 2,6-dichlorophenyl phenyl ring of the diclofenac sodium is attributed to 6.924–6.886 ppm and it is shifted upon its coordination of the silver ion, at 7.001–6.970 (**1**) and 7.072–7.040 (**2**) ppm (Figs. S9–S10). The resonance signals at 6.736–6.699 and 6.231–6.212 ppm respectively are assigned to the H[^{6}C] and the H[^{4}C] protons of the phenyl acetate ring of diclofenac. These signals are shifted in the spectra of **1–2** at 6.812–6.783 and 6.298–6.283 ppm (**1**) and at 6.811–6.782 and 6.286–6.270 ppm (**2**) (Figs. S9–S10). Moreover, the aromatic protons of TPP which are appeared at 7.378–7.171 ppm in the free ligand [2], they are shifted at 7.474–7.449 and 7.354–7.332 ppm upon its coordination on silver ion in the spectrum of **2** (Fig. S10). The signal of H[^{8}C] of the methylene group (−CH_2–) of diclofenac sodium is observed at 3.346 ppm and it is

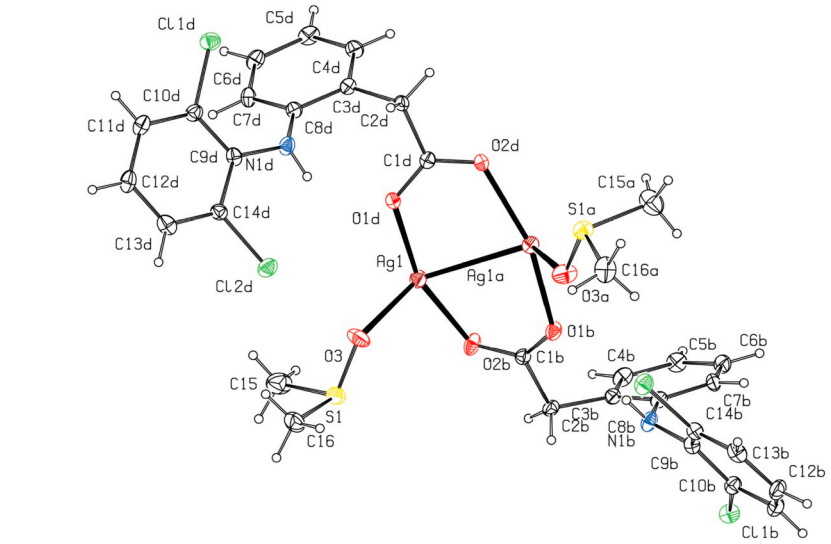

(A)

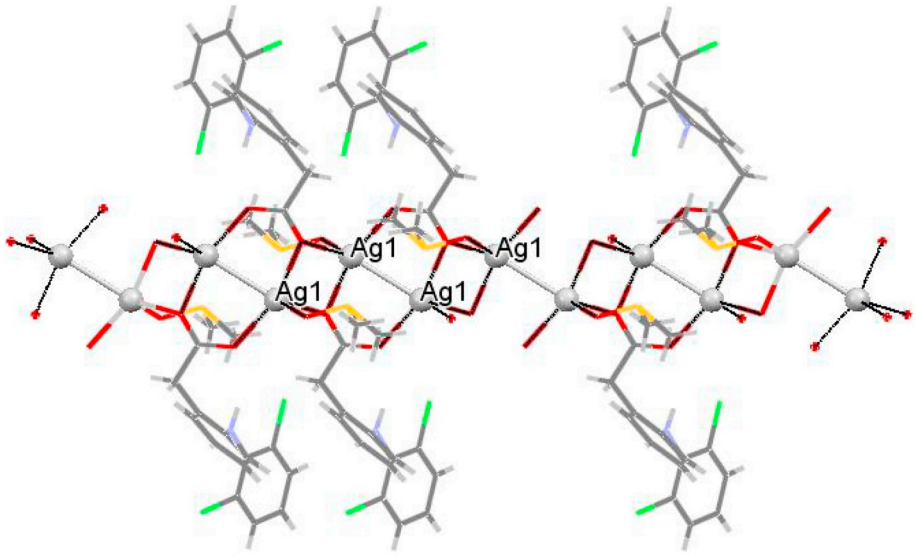

(B)

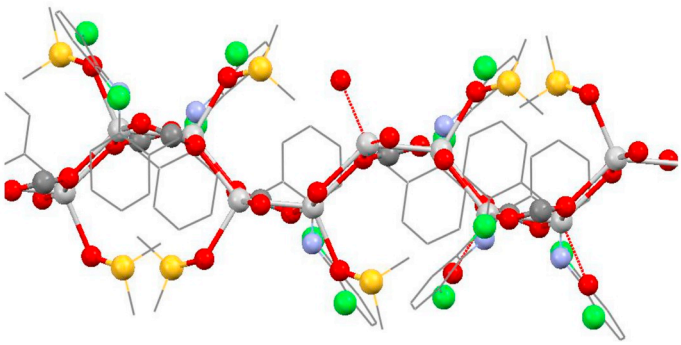

(C)

Fig. 1. (A) ORTEP diagram together with the numbering of **1**. Ag1-O3 = 2.456(5), Ag1-Ag1_a = 2.8451(11), Ag1-O2_b = 2.260(4), Ag1-O1_d = 2.218(4), O1-C1 = 1.258(7), O2-C1 = 1.248(7), O2-Ag1-O3 = 107.32(15), Ag1_a-Ag1-O2 = 132.28(10), O2-Ag1-O2_b = 78.33(15), O1_d-Ag1-O3 = 90.07(17), Ag1_a-Ag1-O2_b = 80.16(10), Ag1_a-Ag1-O1_d = 81.87(10), O1_d-Ag1-O2_b = 161.13(15) (B) Eight member rings as building blogs in the polymeric conformation of **1**. **(C)** A waveform ribbon architecture established due to secondary Ag···O#. Symmetry codes used: a = 1-x,y,3/2-z, b = 1-x,2-y,1-z, d = x,2-y,1/2 + z.

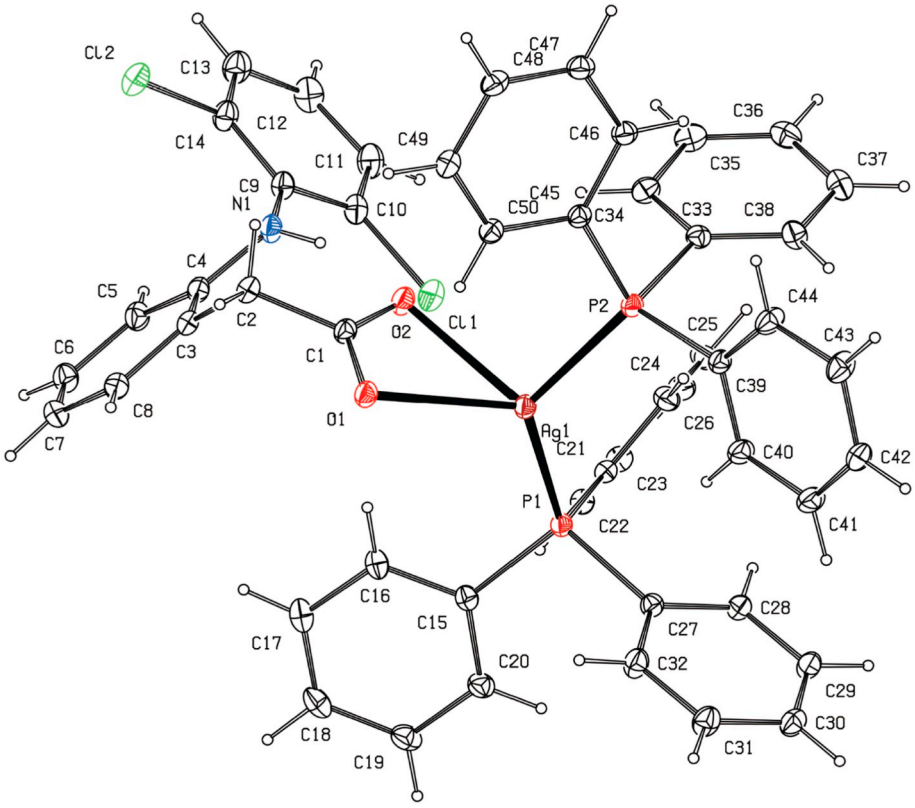

Fig. 2. ORTEP diagram together with the numbering of **2**. Ag1-P1 = 2.4147(6), Ag1-P2 = 2.4322(6), Ag1-O1 = 2.4208(15), Ag1-O2 = 2.4778(16), O1-C1 = 1.258(3), O2-C1 = 1.257(3), P1-Ag1-P2 = 128.25(2), P1-Ag1-O1 = 118.29(4), P1-Ag1-O2 = 110.88(4), P2-Ag1-O1 = 113.05(4), P2-Ag1-O2 = 104.15(4), O1-Ag1-O2 = 53.31(5), O1-C1-O2 = 121.8(2).

shifted in the case of **1** at 3.548 and in the case of **2** at 3.521 ppm (Figs. S9–S10). The strong shift which undergoes these protons indicates the coordination of the ligand to the silver ion through of the carboxylic group [−COOH]. The signal H[CH_3–] of the coordinated DMSO (**1**) is observed at 2.550 ppm (Fig. S9).

2.4. Biological tests

2.4.1. Anti-proliferative activity of the metallodrugs

Since hormones receptors (HRs) are expressed in approximately 65% of human breast cancer and they are involved in the development and propagation of the disease the study of their inhibitors is of great interest towards the development of new chemotherapeutics [29]. The antiproliferative activity (IC_{50}) of **1–2** against human breast adenocarcinoma, hormones depended (MCF-7 (HD)) or independent (MDA-MB-231 (HI)) cells, upon their incubation for 48 h were evaluated by Sulforhodamine B (SRB) assay (Table 1).

The IC_{50} values of **1** against MCF-7 (HD) and MDA-MB-231 (HI) cells are 6.8 ± 0.6 and 12.8 ± 0.3 μM respectively, while the corresponding IC_{50} values of **2** are 2.8 ± 0.2 and 2.7 ± 0.2 μM (Table 1). Thus, **1** inhibits the MCF-7 (HD) than MDA-MB-231 (HI) cells selectively, suggesting hormone mimetic behaviour of it. Compound **2** exhibits 2-fold stronger activity against MCF-7 and 5-fold against MDA-MB-231 than **1**. This might be due to the increase lipophilicity induced by TPP in **2**. The activity of **2** is 9-fold better than cisplatin against MDA-MB-231 cells. Thus, the presence of the mitochondriotropic agent TPP increases its cytotoxicity against both cell lines. Both **1–2** exhibit higher activity than their ligands (Table 1).

The IC_{50} values order, against MCF-7 cell, of the heteroleptic silver (I) metallodrugs with NSAIDs and TPP, synthesized from our group, is: {[Ag(NAPR)(TPP)$_3$](H_2O)} < [Ag(p-HO-BZAH)(TPP)$_2$] < [Ag(NIM)(TPP)$_2$] < {[Ag(ASP)(TPP)$_3$](DMF)} = [Ag(SALH)(TPP)$_2$] < **2**, (NAPRH = naproxen, p-HO-BZAH = p-hydroxy-benzoic acid, NIMH = nimesulide, ASPH = aspirin, $SALH_2$ = salicylic acid) suggesting that, the type of the NSAIDs but not the molecular weight, affects the bioactivity of the agent (Table 1).

The toxicity of **1–2** was evaluated against the normal human fetal lung fibroblast (MRC-5) cells. Their therapeutic potency indexes (TPI), which are defined as the IC_{50} of an agent against non-cancerous cells towards its IC_{50} against cancerous cells, [18] reveal that **1** is less toxic against MCF-7 cells. Their TPI values are: 1.6 (**1**) and 1 (**2**) respectively. TPI value > 1 indicates selectivity of the agent against cancerous than normal cells. The TPI values against MDA-MB-231 cells, are 0.9 (**1**) and 1.0 (**2**). The corresponding TPI values of cisplatin against MCF-7 and MDA-MB-231 cells are 0.2 and 0.04 respectively. In order to evaluate the genotoxicity of **1–2** towards cultured MRC-5 cells, the micronucleus (MN) assay was used. The cells were incubated by the metallodrugs at their IC_{50} values. The presence of the micronucleus indicates genetic damage in different cell types, since the micronucleus is formed after the presence of a chemical agent [30–32]. The MN frequency of the untreated cells is 1.1 ± 0.4%. When the MRC-5 cells were treated with **1–2**, the MN frequencies are increased at 3.5 ± 0.4% (**1**) and 2.9 ± 0.3% (**2**) respectively. This indicates that both compounds are causing genetic damage in the normal cells (Fig. S11). Moreover the MN observed in MRC-5 cell cultures when they are treated by cisplatin is 1.6% [2].

2.4.2. Computational study

The presence of TPP in the coordination sphere of Ag(I) in **2** reduces the cytotoxic activity (Table 1). This might be attributed in the higher lipophilicity introduced by TPP (see above). Thus, computations were employed in order to rationalize the influence of the lipophilicity in the activity of the compounds. The results for the compounds **1** and **2** are included in Table 1 and they are compared with those obtained for others members of this homologues series of compounds. The results confirm our assumption about the influence of the lipophilicity on the compound's activities since compounds of higher LogP (higher lipophilicity) exhibit better cytotoxicity (Table 1). Therefore the {[Ag(NAPR)(TPP)$_3$](H_2O)} with the stronger biological activity exhibits the higher lipophilicity (Table 1).

Table 1
Metal complexes with non-antiinflammatory drugs against adenocarcinoma breast cell lines MCF-7 (hormone dependent), MDA-MB 231 (hormone independent) and one normal human fetal lung fibroblast cells (MRC-5 cells).

Compounds	MW	logP	IC_{50} (μM)			TPI		DNA binding constant's			LOX inhibition	Ref
			MCF-7	MDA-MB 231	MRC-5	MCF-7	MDA-MB 231	K_b ($\times 10^4$) M^{-1}	Hyper/ hypochromicity (H)	Percent (H) (%)	IC_{50} (μM)	
$[Ag_2(DICL)_2(DMSO)_2]_n$ (**1**)	481.14	2.54	6.8 ± 0.6	12.8 ± 0.3	11.1 ± 0.1	1.6	0.9	7.0 ± 0.7	Hyper	1.3	28.8	**
$[Ag(DICL)(TPP)_2]$ (**2**)	927.59	12.91	2.8 ± 0.2	2.7 ± 0.2	2.7 ± 0.1	1.0	1.0	8.2 ± 0.3	Hyper	16.7	> 30	**
$[Ag(p\text{-}HO\text{-}BZAH)(TPP)_2]$*	769.50	10.22	1.4 ± 0.4					27.7 ± 7.9	Hyper	36.5	7.6	[16]
$[Ag(SALH)(TPP)_2]$*	769.50	10.22	2.3 ± 0.3		3.1 ± 0.3	1.3		13.3 ± 6.5	Hyper	47.2	2.3	[16]
{$[Ag(ASP)(TPP)_3](DMF)$}*	1146.90	16.36	2.3 ± 0.3		2.9 ± 0.1	1.3		11.0 ± 2.8	Hyper	36.3	7.2	[16]
{$[Ag(NAPR)(TPP)_3](H_2O)$}*	1141.94	17.69	0.7 ± 0.1					32.8 ± 8.5	Hypo	41.2	5.1	[3]
$[Ag(NIM)(TPP)_2]$*	1011.81	11.74	1.0 ± 0.1	2.3 ± 0.1	2.9 ± 0.1	2.9	1.3	20.0 ± 0.0	Hypo	21.0	12.2	[2]
$[Ag(NIM)(TPTP)_2]$	1023.87	13.48	3.8 ± 0.2	4.4 ± 0.1	6.6 ± 0.1	1.7	1.5	86.2 ± 27.0	Hypo	4.0	5.8	[2]
[Ag(NIM)(TOTP)]	719.53	7.57	2.7 ± 0.1	3.3 ± 0.1	3.1 ± 0.1	1.1	0.9	12.5 ± 4.9	Hypo	8.0	10.8	[2]
$[Ag(NAPR)(TPTP)_2]$	946.88	14.74	2.2 ± 0.2	–	–	–	–	4.7 ± 1.8	Hypo	12.1	> 30	[3]
$[Ag(SALH)(TPTP)_2]$	853.68	13.03	1.7 ± 0.3	–	–	–	–	7.2 ± 1.1	Hypo	10.0	> 30	[4]
$[Ag(SALH)(TMTP)_2]$	853.68	13.03	5.9 ± 0.8	–	–	–	–	5.3 ± 0.8	Hypo	22.0	> 30	[4]
$[Ag(p\text{-}HO\text{-}BZAH)(TPTP)_2]$	853.68	14.28	1.0 ± 0.1					14.6 ± 4.1	Hyper	35.0	> 30	[4]
TPP			28.9 ± 1.4	> 30	> 30	–	–					[2]
Diclofenac Sodium			> 30	> 30	> 30	–	–					**
Cisplatin	300.01		5.5 ± 0.4	26.7 ± 1.1	1.1 ± 0.2	0.2	0.04		–	–	65.9	[2]

**this work, *p-HO-BZAH = p-hydroxy-benzoic acid, $SALH_2$ = salicylic acid, ASPH = aspirin, NAPRH = naproxen, NIMH = nimesulide, TPTP = tri(p-tolyl)phosphine, TOTP = tri(o-tolyl)phosphine, TMTP = Tri(m-tolyl)phosphine.

*2.4.3. Cell migration assay, anti-metastatic potential of **1–2***

Cell migration can be occurred during physiological and pathological processes, and plays an important role in the progression of various diseases [32]. During metastasis the spread and invasion of tumor cells, into host tissues, is initially facilitated by collagenolytic enzymes and is then followed by their migration [33]. Therefore, the assay of the cell migration is essential for the ant-metastatic potency of a metallodrug [34].

In order to investigate the anti-metastatic capacity of **1–2**, their inhibitory activity of MCF-7 cell migration, is studied. Thus, MCF-7 cells were cultured in a six-well plate in culture medium and a scratch was introduced on each well, with a sterilized micro-tip to create gap (wound area) [34]. The cells were then treated with **1–2** and cisplatin at the concentration of 0.2 μM for 48 h. The tested concentration was lower than their IC_{50} values and it is not cytotoxic to the cells. The cell migration was quantified by measuring the gap surface after 48 h. In the untreated MCF-7 cells, the gap was healed up to 20.0 ± 2.4% after 48 h. The treated cells, on the other hand, covered up to 12.4 ± 3.0% of open wound area in the case of **1** and 17.7 ± 2.1% for **2**. Migration calculations revealed that both complexes slowed down the migration of MCF-7 cells effectively. Thereby, they are displaying effective anti-metastatic activity in vitro. Cisplatin, on the other hand, causes cell migration at the same rate at those of the untreated cells (21.0 ± 3.6%). The quantitative values of the wound size as determined by the Image J software are graphically depicted in Fig. 3.

*2.5. Mechanism of action of **1–2***

2.5.1. Cell cycle arrest

In order to test the effect of the cell cycle progression of MCF-7 cells, upon their treatment with **1–2**, flow cytometric analysis was performed. Moreover, sub-G_1 peak on DNA frequency histograms shows the percentage of MCF-7 cells which undergoes apoptosis [35,36]. Fig. 4 illustrates the percentage of MCF-7 cells on the cell cycle, exposed with the metallodrugs **1–2** at concentrations of their IC_{50} values for 48 h. The results are presented as the number of cells versus DNA content in different phases of cell cycle (sub-G_1, G_0/G1, S, and G_2/M).

The untreated cells are spread in 6.10% sub-G_1 phase, 46.50% in G_0/G_1, 18.30% in S and 28.90% in G_2/M phases. Upon treatment of MCF-7 cells with the **1–2**, the cells in the sub-G_1 phase are increased at 18.30% (**1**) and at 12.90% (**2**) respectively, suggesting induction of apoptosis to the cells. Moreover in the case of **1**, the population of cells in the S phase is increased at 29.60% towards the untreated cells (18.30%). As a consequence apoptosis is induced by suppressing the cell proliferation due to DNA synthesis inhibition. This is in accordance with the mechanism proposed for other anticancer agents (mitomycin C, hydroxyurea, resveratrol) [37], silver(I) complexes of nimesulide [2] or NSAID's-silver(I) metallodrugs of salicylic acid and naproxen [18]. However, no such conclusion withdrawn for **2**, where a meaningless variation in G_0/G_1 phase was observed. This slight increasing is due to DNA damage of MCF-7 cells [38]. In any case the apoptosis was concluded, clearly, from the increasing of the peak of sub-G_1 phase.

Cisplatin causes cell cycle arrest either in S or in G_2/M phase, depending on both p53 status and drug concentration [39] and induces apoptosis by increasing the percentage of the MCF-7 cells in the sub-G_1 phase [2]. Thus, **1** acts with a similar manner than cisplatin, and it causes cell cycle arrest in S phase.

2.5.2. Detection of the loss of the mitochondrial membrane permeabilization (MMP assay)

One of the preferable targeting organelle, of tumor cells, in cancer chemotherapy is the mitochondria, nowadays. The mitochondria are involved in the activation of caspases through the releasing of cytochrome *c* in the cytosol and the loss of mitochondrial membrane permeability simultaneously, inducing apoptosis [40,41]. Silver metallodrugs with mitochondriotropic agents, such as triarylphosphines, are causing loss of the mitochondrial permeability resulting in the activation of the intrinsic or mitochondrial pathway of apoptosis [2,18].

The MMP assay is based on the cationic hydrophobic mitochondrial potential dye which is accumulated in mitochondria in the case of the untreated cells. However, when the cells are treated with a metalloagent, the mitochondrial membrane permeability collapses and the fluorescence emission of the dye is decreasing simultaneously.

In order to evaluate the loss of the MMP, the MCF-7 cells were treated with **1–2** at their IC_{50} values, for 48 h, and the fluorescence of the dye is decreasing by 6.5 (**1**) and 11.2 (**2**) % respectively. It is noteworthy that the presence of the TPP enhances, up to 2-fold, the MMP in case of **2**. This is due to the dissolution of the triphenylphosphonium ($TPPH^+$) in mitochondrial membrane because of its high lipophilicity and its stable cationic charge [12]. Generally, the percent of the

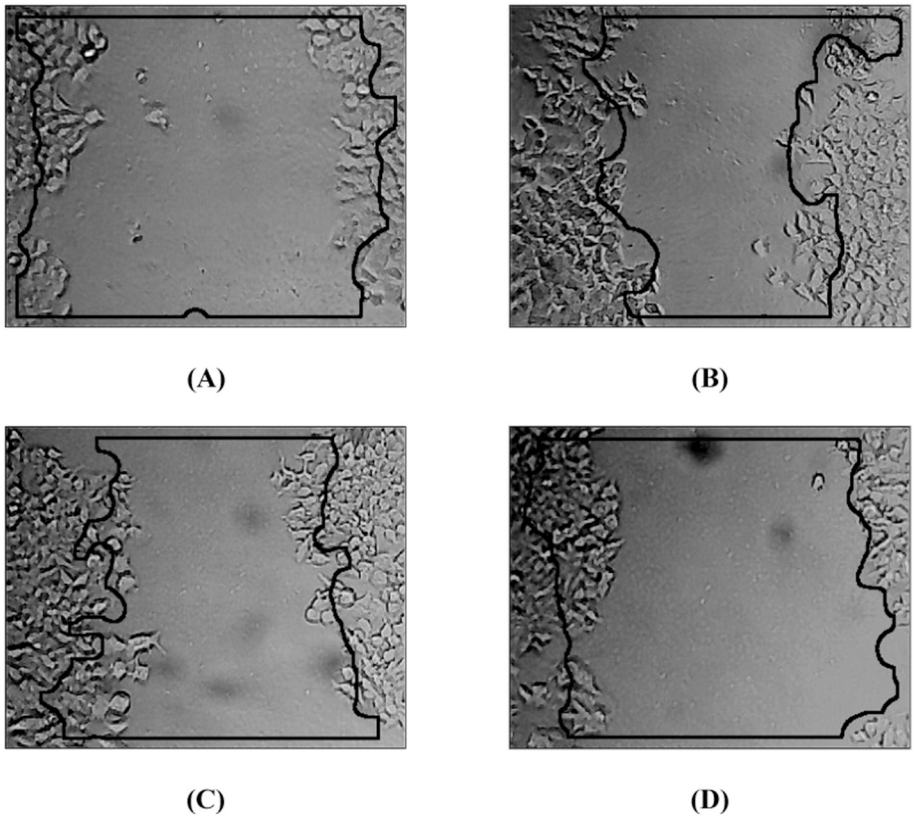

Fig. 3. Overlapping of initial scratch (0 h solid line) and after 48 h showing the MCF-7 migratory pattern: (A) in untreated cells, (B) **1** at 0 2 μM, (C) **2** at 0.2 μM, (D) cisplatin at 0. 2 μM.

decreasing of the fluorescence, in case of **1–2**, is similar with that of {[Ag(NIM)(TPP)$_2$]DMF} (nim = nimesulide, DMF = dimethylformamide), which is already studied from our group previously. In this compound the % decreasing in the fluorescent intense is 15.7%. These results suggest that not only the mitochondriotropic ligand affects the loss of MMP but the type of NSAID as well. Moreover, when the MCF-7 cells are treated with cisplatin at 5.5 μM (IC_{50} value) the fluorescence of the MMP assay dye is decreasing by 54.9% [20]. These values indicate that the mitochondrion-mediated pathway could be participated in the apoptosis of MCF-7 cells in a lower extent, however, than cisplatin.

2.5.3. DNA binding studies

DNA binding studies with the **1–2** were performed by UV absorption spectroscopy to light their mechanism of action inside the cell. Metal complexes bind to DNA through either covalent bond and/or through non-covalent interactions. These interactions include, electrostatic or groove binding of complexes to DNA [16].

Upon the increasing of r values (r = [complex] / [DNA], [DNA] = 10^{-4} M) of the **1–2** a slight increasing in the absorption intensity (at λ_{max} = 258 nm) is observed Fig. S12). The percent of hyperchromicity is calculated 1.3% (**1**) and 16.7% (**2**), respectively for **1–2**. These data suggest breakage of the hydrogen bonds which stabilized the secondary structure of DNA.

Moreover, the binding constants of **1–2** towards CT-DNA were evaluated at 300–310 nm, by monitoring the changes in absorbance of the UV spectra of **1–2**, ([**1**] = 50 μM and [**2**] = 25 μM) with increasing concentration of CT-DNA ([CT-DNA = 10–100 μM) (Fig. S13). The binding constant (K_b) is obtained from the ratio of the slope to the y intercept in plots [DNA] / ($\varepsilon_a - \varepsilon_f$) versus [DNA] [16].

The K_b constants of **1–2** are $(7.0 \pm 0.7) \times 10^4$ and $(8.2 \pm 0.3) \times 10^4\ M^{-1}$, respectively. The K_b value of **2**, which contains TPP, is higher than that of **1**. However, both **1–2** exhibit the lower K_b values among the corresponding silver compounds of NSAIDs, such as aspirin, salicylic acid, naproxen or nimesulide (Table 1). In comparison with other metal complexes compounds of DICLH, **1–2** possess higher K_b ([Cu(dicl)$_2$(phen)] (phen = 1,10-phenanthroline) ($K_b = 1.8 \times 10^4\ M^{-1}$) and [Cu(dicl)$_2(py)_2$] (py = pyridine) ($K_b = 0.4 \times 10^4\ M^{-1}$)) [42].

2.5.4. Study of the lipoxygenase (LOX) inhibition by 1–2

The ability of **1–2** to anchor into mitochondria, initiating cell apoptosis, their LOX inhibitory activity was evaluated. LOX is mainly distributed in mitochondria and it takes part in the mechanism of inflammation, while its inhibition, is induced apoptosis through mitochondrial pathway [2,18,20]. The influence of the metallodrugs on the LOX in a concentration range of 10–40 μM was studied by monitoring the hyperoxy linoleic acid formed, as described elsewhere (Fig. S14) [43]. The IC_{50} value of **1** is 28.8 μM, while the corresponding one of **2** is higher than 30 μM. The IC_{50} value of sodium diclofenac is also higher than 30 μM. Silver compounds of NSAIDs, such as nimesulide, naproxen, aspirin and salicylic acid and TPP, exhibit a range of IC_{50} value against LOX of 2.3 to 12.2 μM [18] (Table 1). Generally, compounds with strong inhibitory activity against LOX also exhibit strong anti-proliferative activity against cancerous cells (Table 1). This data indicate that the inhibition activity of the enzyme lipoxygenase is also be affected by the presence of the NSAID.

2.5.5. Multivariable regression analysis

A regression analysis for the compounds shown in Table 1 is attempted, in an effort to determine a simple model that can describe the pIC_{50} (dependent variable) as a function of pK_b, logP and log(MW) (independent variables). Since the number of samples was lower than 50 we used all of them in the modeling and checked the model by leave-one-out cross-validation (LOOCV) technique [44]. The analysis was done in Python version 3.6.5 with thesklearn.linear_model.Ridge package from the machine learning package scikit-learn [45]. Ordinary

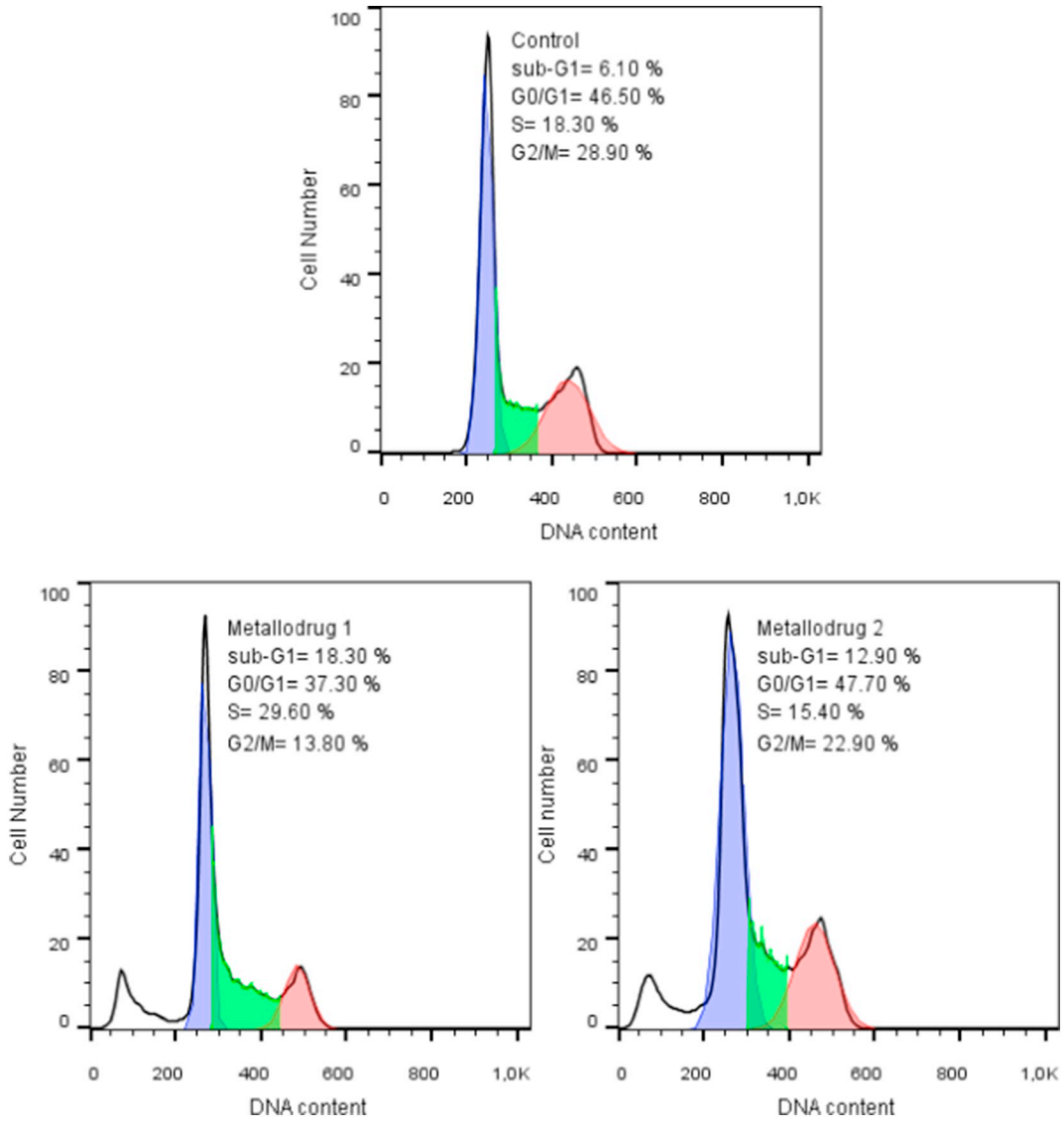

Fig. 4. Effects of the metallodrugs **1–2** on cell cycle against MCF-7 cells. The relative number of cells within each cell cycle was determined by flow cytometry. Number of cells in sub-G_1, G_0/G_1, S and G_2/M phases are indicated.

least squares (OLS) is shown to be prone to overfitting; our initial test with OLS yielded an R-squared value of 0.99 which confirmed that disadvantage. Ridge regression (RS) on the other hand, performs L2 regularization to the data by adding a factor of sum of squares of coefficients in the optimization function [46]. In RS the cost function (residual sum of squares) that has to be minimized is:

$$W = \left[\sum_{i=1}^{m} |y_i - \hat{y}_i|^2 + \lambda \sum_{j=1}^{n} \theta_j^2 \right]$$

where, m is the number of observations, $\hat{y}$ is the predicted value, y is the true value of the response, λ is a regularization parameter multiplied with the sum of square of the magnitude of weights, and θ is the norm of the coefficients. The first term represents the normal cost function of OLS; the second term penalizes big coefficients by pulling them towards zero. This process decreases the variance in the model, avoids overfitting, and leads to better predictions. λ is a tuning parameter, which controls the strength of the penalty term. Since there is no way to know beforehand the best value for λ (with $\lambda > 0$), we cross-validated different models with different λs and choose the one with the least prediction error. In Fig. 5 the two extremes of the graph denote model underfitting (high λ) and model overfitting (low λ). As a result, we performed ridge regression modeling using LOOCV in the log space $(-5, 1)$ to optimize λ, and concluded to the following model:

$$\mathbf{pIC_{50} = -0.24 * pK_b + 0.04 * logP - 0.52 * log(MW) + 5.37} \quad (2)$$

where $IC_{50} = -\log(IC_{50})$, K_b = DNA binding constant, logP = the octanol / water partition coefficient and MW = molecular weight.

Fig. 6 depicts the regression model along with the residuals. The latter form a randomly scattered pattern around zero, indicating a reliable model.

3. Conclusion

The Conjugation of Metals (e.g. silver etc.) with specific classes of Drugs such as NSAIDs, (CoMeD's) enhances their activity, due to synergistic effect. The CoMeDs display a range of biological potency inaccessible to the original ligands [7]. Moreover, hormones receptors are expressed in human breast cancer and they are involved in the development and propagation of the disease. The study of their inhibitors therefore is of great interest towards the development of new treatment's strategist and cancer chemotherapeutics [29].

Compound **1** inhibits MCF-7 (HD) than MDA-MB-231 (HI) cells selectively, while **2**, both cancerous cell lines. The presence of the

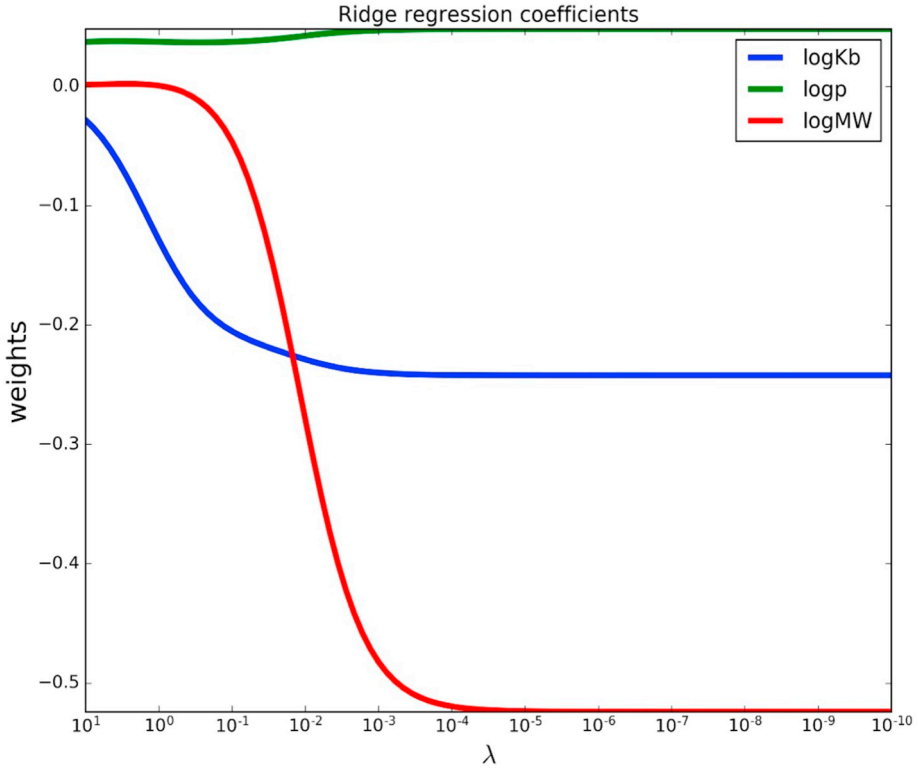

Fig. 5. Ridge regression coefficients as a function of regularization. (For interpretation of the references to color in this figure, the reader is referred to the web version of this article.)

mitochondriotropic agent TPP in **2** increases its cytotoxicity against both cell lines. Both, **1** and **2** inhibit MCF-7 cancer cells migration, by delaying it at 1/2 or 3/4 in respect of the control cells. This is an essential characteristic of anti-metastatic agents.

Among heteroleptic silver compounds of NSAID's and triarylphosphines the {[Ag(NAPR)(TPP)$_3$](H$_2$O)} one, with (i) the higher intercalative binding affinity towards DNA, (ii) the higher lipophilicity calculated and (iii) the stronger LOX inhibitory activity shows the stronger antiproliferation activity against MCF-7 (Table 1). The activity of **2** lies at the upper borderline. Regression analysis leads to the Eq. (2) which correlates the pIC$_{50}$ calculation as a function of pK$_b$, logP and log (MW). Eq. (2) creates IC$_{50}$ values which fit well with the experimental ones. Finally, the high success of the Eq. (2), throw light on significance of theses parameters on cells chemistry regulation.

4. Experimental

4.1. Materials and instruments

All solvents used were of reagent grade. Solvents used were of reagent grade, while triphenylphosphine (Sigma-Aldrich, Merck) was used without further purification. Dulbecco's modified Eagle's medium, (DMEM), fetal bovine serum, glutamine and trypsin were purchased from Gibco, Glasgow, UK. Phosphate buffer saline (PBS), CT-DNA, propidium iodide, RNase A, Proteinase K were purchased from Sigma-Aldrich. Dimethyl sulfoxide and boric acid were from Riedel-de Haen. Melting points were measured in open tubes with a Stuart Scientific apparatus and are uncorrected. IR spectra in the region of 4000–370 cm^{-1} were obtained from KBr discs, with a Perkin-Elmer

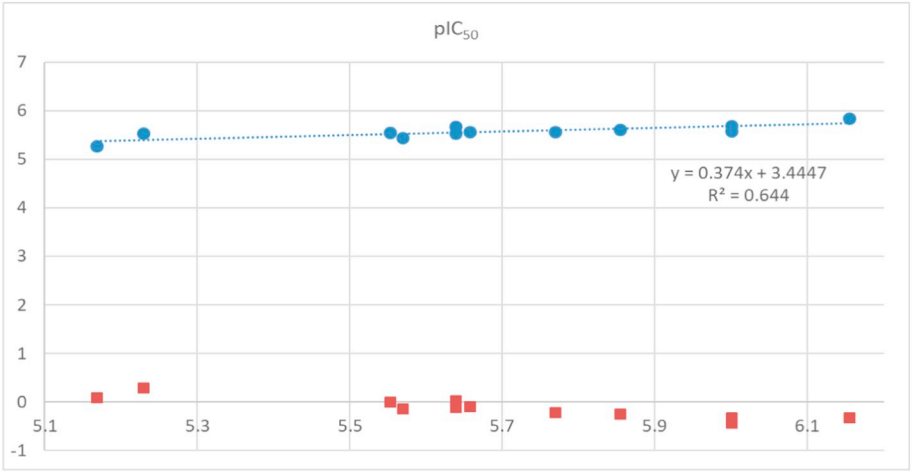

Fig. 6. Ridge regression fitting (circles) and residuals (squares). (For interpretation of the references to color in this figure, the reader is referred to the web version of this article.)

Spectrum GX FT-IR spectrophotometer. The ^{1}H NMR spectra were recorded on a Bruker AC 400 MHz FT-NMR instrument in DMSO-d_6 solution. A UV-1600 PC series spectrophotometer of VWR was used to obtain electronic absorption spectra. FACS Calibur flow cytometer (Becton Dickinson, San Jose, CA, USA) was obtained for the cell cycle.

4.2. Synthesis and crystallization of 1–2

0.185 g of diclofenac diethylamine (0.5 mmol) and 0.085 g silver nitrate (0.5 mmol) were stirred in DMSO (5 mL) at room temperature. The mixture was stirred for 30 min and the solution was kept in darkness. Colourless crystals of **1** were grown from the solution and they were filtered off and dry under vacuum over calcium chloride. 0.241 g of **1** (0.5 mmol) were dissolved in DMSO (10 mL), and 0.256 g triphenylphosphine (1 mmol) were added afterwards. The mixture was stirred for 30 min and the solution was kept in darkness. Colourless crystals of **2** were filtered off and dry under vacuum over calcium chloride after 2 days.

1: white crystal, melting point: 130–135 °C; elemental analysis found: C: 39.90; H: 3.22, N: 2.88, S: 6.57%; calculated for $C_{16}H_{16}AgCl_2N_1O_3S_1$: C: 39.94; H: 3.35, N: 2.91, S: 6.66%. IR (cm^{-1}), (KBr): 1577 vs, 1556 vs, 1504 vs, 1465 m, 1453 vs, 1381 s, 1305 w, 1290 w, 1248 w, 1197 w, 1154 m, 1022 w, 949 m, 868 m, 837 s, 765 s, 744 vs, 714 s; ^{1}H NMR (ppm) in DMSO-d_6: 9.193 (s, H-N), 7.487–7.471 (d, H(^{1,3}C)), 7.134–7.088 (m, H(^{5,7}C)), at 7.001–6.970 (t, H(^{2}C)), 6.812–6.783 (m, H(^{6}C)), 6.298–6.283 (m, H(^{4}C)), 3.548 (s, H(^{8}C)); UV–vis (DMSO): λ = 291 nm (logε = 4.07).

2: white crystal, melting point: 198–200 °C; elemental analysis found: C: 64.95; H: 4.01, N: 1.65%; calculated for $C_{50}H_{40}AgCl_2N_1O_2P_2$: C: 64.75; H: 4.35, N: 1.51%. IR (cm^{-1}), (KBr): 1555 s, 1571 vs, 1478 s, 1452 s, 1436 vs, 1384 s, 1307 m, 1275 m, 1156 m, 1097 s, 995m, 926 w, 852 w, 745 vs, 691 vs, 650 m, 511 s, 493 s; ^{1}H NMR (ppm) in DMSO-d_6: 9.745 (H-N), 7.421–7.405 (H(^{1,3}C)), 7.421–7.405 (H(^{1,3}C)), 7.116–7.106 (H(^{5,7}C)), 7.072–7.040 (H(^{2}C)), 6.811–6.782 (H(^{6}C)), 6.286–6.270 (H(^{4}C)), 3.521 (H(^{8}C)), 7.474–7.449 (aromatics of protons of the TPP) 7.354–7.332 (aromatics of protons of the TPP); UV–vis (DMSO): λ = 275 nm (logε = 4.41).

4.3. X-ray structure determination

Single crystals of **1–2**, suitable for crystal structure analysis were obtained by slow evaporation of their mother liquids at room temperature. They were mounted at room temperature on a Bruker Kappa APEX2 diffractometer equipped with a triumph monochromator using MoKα radiation. Unit cell dimensions were determined and refined by using the angular settings of at least 200 high intensity reflections (> 10 σ(I)) in the range 2.9 < 2θ < 27.2°. Intensity data were recorded using φ and ω scans. All crystals presented no decay during the data collection. The frames collected for each crystal were integrated with the Bruker SAINT Software package [47] using a narrow–frame algorithm. Data were corrected for absorption using the numerical method (SADABS) based on crystal dimensions [48]. The structures were solved using the SUPERFLIP package [49] incorporated in Crystals. Data refinement (full–matrix least–squares methods on F^2) and all subsequent calculations were carried out using the Crystals version 14.40b program package All non–hydrogen atoms were refined anisotropically. Hydrogen atoms were located by difference maps at their expected positions and refined using soft constraints. By the end of the refinement, they were positioned geometrically using riding constraints to bonded atoms.

1: $C_{16}H_{16}AgCl_2N_1O_3S_1$, MW = 481.11, monoclinic, space group C2/c, a = 36.932(11), b = 9.577(3), c = 9.898(3) Å, α = 90, β = 96.670(8), γ = 90°, V = 3477.2(18) Å^3, Z = 8, T = 295 K, ρ (calc) = 1.838 g cm^{-3}, μ = 1.601 mm^{-1}, F(000) = 1920. 22,748 reflections measured, 3842 unique (Rint = 0.085). The final R1 = 0.0448 (for 2244 reflections with I > 2s(I)) and wR(F2) = 0.0993 (all data) S = 1.00.

2: $C_{50}H_{40}AgCl_2N_1O_2P_2$, MW = 927.55, monoclinic, space group P21/n, a = 18.3746(10), b = 10.8666(6), c = 22.2924(12) Å, α = 90, β = 91.0196(18), γ = 90°, V = 4450.4(4) Å^3, Z = 4, T = 295 K, ρ (calc) = 1.384 g cm^{-3}, μ = 0.685 mm^{-1}, F(000) = 1896. 72,866 reflections measured, 8842 unique (Rint = 0.023). The final R1 = 0.0241 (for 5847 reflections with I > 2s(I)) and wR(F2) = 0.0433 (all data) S = 1.00.

Crystallographic data (excluding structure factors) for the structures reported in this paper have been deposited with the Cambridge Crystallographic Data Centre as supplementary publication no. CCDC-1872934 (**1**), 1872935 (**2**). Copies of the data can be obtained free of charge on application to CCDC, 12 Union Road, Cambridge CB2 1EZ, UK (fax: (+44) 1223-336-033; e-mail: deposit@ccdc.cam.ac.uk).

4.4. Biological tests

4.4.1. Solvents used

Stock solutions of complexes **1–2** (0.01 M) in DMSO were freshly prepared and diluted with cell culture medium to the desired concentration. The biological experiments including the SRB assay, cell morphology, cell cycle, micronucleus and the permeabilization of mitochondrial membrane were carried in DMSO/DMEM solutions 0.0051–0.1% v/v DMSO in DMEM for **1–2**. For DNA binding studies and LOX inhibition, the experiments were carried in DMSO/buffer solutions (0.00025–0.005% v/v DMSO).

SRB assay, Micronucleus, Cell morphology, Cell cycle, Detection of the loss of the Mitochondrial Membrane Permeabilization, DNA binding studies and Study of the peroxidation of linoleic acid by the enzyme lipoxygenase were performed in accordance with the previous reported method [2,18].

4.4.2. Determination of lipophilicity

Lipophilicity determination was performed using the Marvin software ver. 16.7.25.0 by ChemAxon release at 2016, based on the crystal structures.

Abbreviations

Ar3P	Triarylphosphines
ASPH	Aspirin
CoMeD	Conjugation of Metals with specific classes of Drugs
CT-DNA	Calf Thymus DNA
DICLH	Diclofenac
DMF	Dimethylformamide
DMSO	Dimethyl sulfoxide
Kb	DNA binding Constant
logP	Octanol/water partition coefficient
LOX	Lipoxygenase
MCF-7	Human breast adenocarcinoma cells - hormone dependent
MDA-MB-231	Human breast adenocarcinoma cells - hormone independent
MMP assay	Mitochondrial Membrane Permeabilization assay
MRC-5	Fetal lung fibroblast cells
MW	Molecular weight
NAPRH	Naproxen
NIM	Nimesulide
NSAID	Non-Steroidal Anti-inflammatory Drug
OLS	Ordinary least squares
phen =	1,10-phenanthroline
p-HO-BZAH	p-hydroxy-benzoic acid
py =	Pyridine
RS	Ridge regression
SALH2	Salicylic acid
SRB assay	Sulforhodamine B assay
TMTP	Tri(m-tolyl)phosphine

TOTP	Tri(o-tolyl)phosphine
TPI =	Therapeutic potency index
TPP =	Triphenylphosphine
TPPH +	Triphenylphosphonium
TPTP	Tri(p-tolyl)phosphine
Ar3P	Triarylphosphines

Acknowledgements

(i) Diclofenac diethylamine and sodium diclofenac were provided from Help Pharmaceutical, which is acknowledged (ii) The Unit of Bioactivity Testing of Xenobiotics, of the University of Ioannina, for providing access to the facilities is also acknowledged. (iii) The Atherothrombosis Research Centre of the University of Ioannina provides access to the flow cytometer and to the fluorescence microscopy, (iv) The International Graduate Program in "Biological Inorganic Chemistry", which operates at the University of Ioannina within the collaboration of the Departments of Chemistry of the Universities of Ioannina, Athens, Thessaloniki, Patras, Crete, and the Department of Chemistry of the University of Cyprus, is acknowledged for the stimulating discussions.

Appendix A. Supplementary data

Supplementary data to this article can be found online at https://doi.org/10.1016/j.jinorgbio.2019.01.020.

References

[1] P.C. Elwood, A.M. Gallagher, G.G. Duthie, L.A.J. Mur, G. Morgan, Aspirin, salicylates, and cancer, Lancet 373 (2009) 1301–1309.
[2] C.N. Banti, C. Papatriantafyllopoulou, M. Manoli, A.J. Tasiopoulos, S.K. Hadjikakou, Nimesulide silver metallodrugs, containing the mitochondriotropic, triaryl derivatives of pnictogen; anticancer activity against human breast cancer cells, Inorg. Chem. 55 (2016) 8681–8696.
[3] C.N. Banti, A.D. Giannoulis, N. Kourkoumelis, A. Owczarzak, M. Kubicki, S.K. Hadjikakou, Novel metallo-therapeutics of the NSAID naproxen. Interaction with intracellular components that leads the cells to apoptosis, Dalton Trans. 43 (2014) 6848–6863.
[4] C.N. Banti, A.D. Giannoulis, N. Kourkoumelis, A.M. Owczarzak, M. Kubicki, S.K. Hadjikakou, Silver(I) metallo-drugs of anti-inflammatory agents salicylic acid and its derivative which modulate cells function, J. Inorg. Biochem. 142 (2015) 132–144.
[5] E. Gottfried, S.A. Lang, K. Renner, A. Bosserhoff, W. Gronwald, M. Rehli, S. Einhell, I. Gedig, K. Singer, A. Seilbeck, A. Mackensen, O. Grauer, P. Hau, K. Dettmer, R. Andreesen, P.J. Oefner, M. Kreutz, New aspects of an old drug – diclofenac targets MYC and glucose metabolism in tumor cells, PLoS One 8 (2013) e66987.
[6] R. Moreno-Sanchez, C. Bravo, C. Vasquez, G. Ayala, L.H. Silveira, M. Martınez-Lavın, Inhibition and uncoupling of oxidative Phosphorylation by nonsteroidal anti-inflammatory drugs, study in mitochondria, submitochondrial particles, cells, and whole hear, Biochem. Pharmacol. 57 (1999) 743–752.
[7] C.N. Banti, S.K. Hadjikakou, Functionalized nonsteroidal anti-inflammatory drugs (NSAIDs) by metal ions with involvement on the cellular level, Eur. J. Inorg. Chem. (2016) 3048–3071.
[8] C.N. Banti, S.K. Hadjikakou, Anti-proliferative and anti-tumor activity of silver(I) compounds, Metallomics 5 (2013) 569–596.
[9] F.K. Braun, N. Al-Yacoub, M. Plotz, Markus Mobs, W. Sterry, J. Eberle, Nonsteroidal anti-inflammatory drugs induce apoptosis in cutaneous T-cell lymphoma cells and enhance their sensitivity for TNF-related apoptosis-inducing ligand, J. Invest. Dermatol. 132 (2012) 429–439.
[10] J.M. Stelzer, J.L. Colaizzi, P.J. Wurdack, Influence of dimetylsulfoxide (DMSO) on the percutaneous absorption of salicylic acid and sodium salicylate from ointments, J. Pharm. Sci. 57 (1968) 1732–1737.
[11] A. Horita, L.J. Weber, Skin penetrating property of drugs dissolved in dimethylsulfobide (DMSO) and other vehicles, Life Sci. 3 (1964) 1389–1395.
[12] M. Han, M.R. Vakili, H. Soleymani Abyaneh, O. Molavi, R. Lai, A. Lavasanifar, Mitochondrial delivery of doxorubicin via triphenylphosphine modification for overcoming drug resistance in MDA-MB-435/DOX cells, Mol. Pharm. 11 (2014) 2640–2649.
[13] S. Savino, C. Marzano, V. Gandin, J.D. Hoeschele, G. Natile, N. Margiotta, Multi-acting mitochondria-targeted platinum(IV)prodrugs of kiteplatin with -lipoic acid in the axial positions, Int. J. Mol. Sci. 19 (2018) 2050–2066.
[14] S. Savino, V. Gandin, J.D. Hoeschele, C. Marzano, G. Natile, N. Margiotta, Dual-acting antitumor Pt(IV) prodrugs of kiteplatin with dichloroacetate axial Ligands, Dalton Trans. 47 (2018) 7144–7158.
[15] M. Poyraz, C.N. Banti, N. Kourkoumelis, V. Dokorou, M.J. Manos, M. Simčič, S. Golič-Grdadolnik, T. Mavromoustakos, A.D. Giannoulis, I.I. Verginadis, K. Charalabopoulos, S.K. Hadjikakou, Synthesis, structural characterization and biological studies of novel mixed ligand Ag(I) complexes with triphenylphosphine and aspirin or salicylic acid, Inorg. Chim. Acta 375 (2011) 114–121.
[16] C.N. Banti, A.D. Giannoulis, N. Kourkoumelis, A.M. Owczarzak, M. Poyraz, M. Kubicki, K. Charalabopoulos, S.K. Hadjikakou, Mixed ligand–silver(I) complexes with anti-inflammatory agents which can bind to lipoxygenase and calf-thymus DNA, modulating their function and inducing apoptosis, Metallomics 4 (2012) 545–560.
[17] E.I. Gkaniatsou, C.N. Banti, N. Kourkoumelis, S. Skoulika, M. Manoli, A.J. Tasiopoulos, S.K. Hadjikakou, Novel mixed metal Ag(I)-Sb (III)-metallotherapeutics of the NSAIDs, aspirin and salicylic acid: enhancement of their solubility and bioactivity by using the surfactant CTAB, J. Inorg. Biochem. 150 (2015) 108–119.
[18] C.N. Banti, C. Papatriantafyllopoulou, A.J. Tasiopoulos, S.K. Hadjikakou, New metalo-therapeutics of NSAIDs against human breast cancer cells, Eur. J. Med. Chem. 143 (2018) 1687–1701.
[19] G.K. Latsis, C.N. Banti, N. Kourkoumelis, C. Papatriantafyllopoulou, N. Panagiotou, A. Tasiopoulos, A. Douvalis, A.G. Kalampounias, T. Bakas, S.K. Hadjikakou, Poly organotin acetates against DNA with possible implementation on human breast cancer, Int. J. Mol. Sci. 19 (2018) 2055–2072.
[20] M.P. Chrysouli, C.N. Banti, N. Kourkoumelis, N. Panayiotou, A.J. Tasiopoulos, S.K. Hadjikakou, Chloro(triphenylphosphine)gold(I) a forefront reagent in gold chemistry as apoptotic agent for cancer cells, J. Inorg. Biochem. 179 (2018) 107–120.
[21] V. Tsiatouras, C.N. Banti, A.M. Grześkiewicz, G. Rossos, N. Kourkoumelis, M. Kubicki, S.K. Hadjikakou, Structural, photolysis and biological studies of novel mixed metal Cu(I)-Sb(III) mixed ligand complexes, J. Photochem. Photobiol. B 163 (2016) 261–268.
[22] M. Arda, I.I. Ozturk, C.N. Banti, N. Kourkoumelis, M. Manoli, A.J. Tasiopoulos, S.K. Hadjikakou, Novel bismuth(III) bromide or iodide compounds; synthesis, characterization and biological activity against human adenocarcinoma cell lines, RSC Adv. 6 (2016) 29026–29044.
[23] L. Yang, D.R. Powell, R.P. Houser, Structural variation in copper(I) complexes with pyridylmethylamide ligands: structural analysis with a new four-coordinate geometry index, τ4, Dalton Trans. (2007) 955–964.
[24] R. Bouchal, I. Miletto, U. Dong Thach, B. Prelot, G. Berlie, P. Hesemann, Ionosilicas as efficient adsorbents for the separation of diclofenac and sulindac from aqueous media, New J. Chem. 40 (2016) 7620–7626.
[25] M.A. Abdellah, S.K. Hadjikakou, N. Hadjiliadis, M. Kubicki, T.Bakas.N. Kourkoumelis, Y.V. Simos, S. Karkabounas, M. Barsan, I.S. Butler, Synthesis, characterization and biological studies of organotin(IV) derivatives with o- or p-hydroxy-benzoic acids, Bioinorg. Chem. Appl. 2009 (2009) 12, https://doi.org/10.1155/2009/542979 542979.
[26] M. Sariisik, M. Arici, Ö. Topbas, S. Yaprak Karavana, C. Öztürk, G. Ertan, Design of orthopedic support material containing diclofenac sodium microparticles: preparation and characterization of microparticles and application to orthopedic support material, Text. Res. J. 83 (2013) 1030–1043.
[27] S. Lobo, H. Li, N. Farhan, G. Yan, Evaluation of diclofenac prodrugs for enhancing transdermal delivery, Drug Dev. Ind. Pharm. 40 (2014) 425–432.
[28] M.S. Refat, G.G. Mohamed, M.Y.S. Ibrahim, H.M.A. Killa, H. Fetooh, Synthesis and characterization of coordination behavior of diclofenac sodium drug toward hg(II), Pb(II), and Sn(II) metal ions: chelation effect on their thermal stability and biological activity, Synth. React. Inorg., Met.-Org., Nano-Met. Chem. 44 (2014) 161–170.
[29] M. Razandi, A. Pedram, E.R. Levin, Plasma membrane estrogen receptors signal to antiapoptosis in breast cancer, Mol. Endocrinol. 14 (2000) 1434–1447.
[30] O. Torres-Bugarín, M.G. Zavala-Cerna, A. Nava, A. Flores-García, M.L. Ramos-Ibarra, Potential uses, limitations, and basic procedures of micronuclei and nuclear abnormalities in buccal cells, Dis. Markers 2014 (2014) 13, https://doi.org/10.1155/2014/956835 956835.
[31] A. Celik, O. Ogenler, U. Comelekoglu, The evaluation of micronucleus frequency by acridine orange fluorescent staining in peripheral blood of rats treated with lead acetate, Mutagenesis 20 (2005) 411–415.
[32] L. Colina-Vegas, L. Luna-Dulcey, A.M. Plutin, E.E. Castellano, M.R. Cominetti, A.A. Batista, Half sandwich Ru(ii)-acylthiourea complexes: DNA/HSA-binding, anti-migration and cell death in a human breast tumor cell line, Dalton Trans. 46 (2017) 12865–12875.
[33] D.E. Woolley, Collagenolytic mechanisms in tumor cell invasion, Cancer Metastasis Rev. 3 (1984) 361–372.
[34] K. Sarkar, S. Khasimbi, S. Mandal, P. Dastidar, Rationally developed metallogelators derived from pyridyl derivatives of NSAIDs displaying anti-inflammatory and anti-cancer activities, ACS Appl. Mater. Interfaces 10 (2018) 30649–30661.
[35] M. Kajstura, H.D. Halicka, J. Pryjma, Z. Darzynkiewicz, Discontinuous fragmentation of nuclear DNA during apoptosis revealed by discrete "sub-G1" peaks on DNA content histograms, Cytometry A 71A (2007) 125–131.
[36] Y. Chen, K. Yu, N.-Y. Tan, R.-H. Qiu, W. Liu, N.-L. Luo, L. Tong, C.-T. Au, Z.-Q. Luo, S.-F. Yin, Synthesis, characterization and anti-proliferative activity of heterocyclic hypervalent organoantimony compounds, Eur. J. Med. Chem. 79 (2014) 391–398.
[37] S.H. van Rijt, I. Romero-Canelon, Y. Fu, S.D. Shnyder, P.J. Sadler, Potent organometallic osmium compounds induce mitochondria-mediated apoptosis and S-phase cell cycle arrest in A549 non-small cell lung cancer cells, Metallomics 6 (2014) 1014–1022.
[38] C.H. Ng, S.M. Kong, Y.L. Tiong, M.J. Maah, N. Sukram, M. Ahmad, A.S. Khoo, Selective anticancer copper(II)-mixed ligand complexes: targeting of ROS and proteasomes, Metallomics 6 (2014) 892–906.
[39] E.A. Kohn, N.D. Ruth, M. Kay Brown, M. Livingstone, A. Eastman, Abrogation of the S phase DNA damage checkpoint results in S phase progression or premature

mitosis depending on the concentration of 7 hydroxystaurosporine and the kinetics of Cdc25C activation, J. Biol. Chem. 277 (2002) 26553–26564.
[40] S.A. Susin, H.K. Lorenzo, N. Zamzami, I. Marzo, B.E. Snow, G.M. Brothers, J. Mangion, E. Jacotot, P. Costantini, M. Loeffler, N. Larochette, D.R. Goodlett, R. Aebersold, D.P. Siderovski, J.M. Penninger, G. Kroemer, Molecular characterization of mitochondrial apoptosis-inducing factor, Nature 397 (1999) 441–446.
[41] L. Zeng, Y. Chen, J. Liu, H. Huang, R. Guan, L. Ji, H. Chao, Ruthenium(II) complexes with 2-phenylimidazo[4,5-f][1,10] phenanthroline derivatives that strongly combat cisplatin-resistant tumor cells, Sci. Rep. 6 (2016) 19449–19462.
[42] F. Dimiza, F. Perdih, V. Tangoulis, I. Turel, D.P. Kessissoglou, G. Psomas, Interaction of copper(II) with the non-steroidal anti-inflammatory drugs naproxen and diclofenac: synthesis, structure, DNA- and albumin-binding, J. Inorg. Biochem. 105 (2011) 476–489.
[43] M.N. Xanthopoulou, S.K. Hadjikakou, N. Hadjiliadis, E.R. Milaeva, J.A. Gracheva, V. Yu Tyurin, N. Kourkoumelis, K.C. Christoforidis, A.K. Metsios, S. Karkabounas, K. Charalabopoulos, Biological studies of new organotin(IV) complexes of thioamide ligands, Eur. J. Med. Chem. 43 (2008) 327–335.
[44] D.M. Hawkins, The problem of overfitting, J. Chem. Inf. Comput. Sci. 44 (2004) 1–12.
[45] F. Pedregosa, G. Varoquaux, A. Gramfort, V. Michel, B. Thirion, O. Grisel, M. Blondel, P. Prettenhofer, R. Weiss, V. Dubourg, J. Vanderplas, A. Passos, D. Cournapeau, scikit-learn: machine learning in python, J. Mach. Learn. Res. (2011) 2825–2830.
[46] W.N. van Wieringen, Lecture Notes on Ridge Regression, arXiv preprint arXiv:1509.09169 (2015).
[47] Bruker Analytical X-ray Systems, Inc, Apex2, Version 2 User Manual, M86–E01078, Madison, WI, (2006).
[48] Siemens Industrial Automation, Inc., SADABS: Area–Detector Absorption Correction; Madison, WI, (1996).
[49] L. Palatinus, G. Chapuis, SUPERFLIP – a computer program for the solution of crystal structures by charge flipping in arbitrary dimensions, J. Appl. Crystallogr. 40 (2007) 786–790.